PCCP

Accepted Manuscript

This article can be cited before page numbers have been issued, to do this please use: A. L. Suherman, G. Zampardi, S. Kuss, E. E. L. Tanner, H. M.A. Amin, N. P. Young and R. G. Compton, *Phys. Chem. Chem. Phys.*, 2018, DOI: 10.1039/C8CP05154B.

View Article Online
DOI: 10.1039/C8CP05154B

PCCP

ARTICLE

Understanding Gold Nanoparticle Dissolution in Cyanide-Containing Solution via Impact-Chemistry

Received 00th January 20xx,
Accepted 00th January 20xx

DOI: 10.1039/x0xx00000x

www.rsc.org/

Alex L. Suherman,[a] Giorgia Zampardi,[a] Sabine Kuss,[a,#] Eden E. L. Tanner,[a,†] Hatem M. A. Amin,[a] Neil P. Young [b] and Richard G. Compton [a]

The electrochemical dissolution of citrate-capped gold nanoparticles (AuNPs) was studied in cyanide (CN^-) containing-solutions. It was found that the gold nanoparticles showed different dissolution behaviour as ensembles than as single particles. At the single particle level, a nearly complete oxidation of 60 nm AuNPs was achieved at concentrations greater than or equal to 35.0 mM CN^- and at a potential of 1.0 V. Mechanistic insights and rate data are reported.

Introduction

Gold nanoparticles have attracted much attention due to their use in catalysis and electrocatalysis[1-3], in electrochemical sensing[4], in medicine as drug delivery systems[5] and as therapeutic agents for cancer treatments[6]. Moreover, the applications have been recently extended to the electrochemical detection and quantification of pathogenic bacteria[7,8]. Nevertheless, much chemistry of gold and gold nanoparticles remains unclear.[9-12] Moreover, the challenges related to the technologies required to synthesize gold nanoparticle, such as cost, environmental impact and toxicity issues, can potentially limit their use.[10,11] To minimize these effects, the recovery or refinery of gold nanoparticles from diverse sources is becoming increasingly important. The recovery of gold nanoparticles from aqueous solutions can be performed using extracting agents such as biogenic-sulphide[13], surfactants[14], polymers[15] and cyanide salts in conjunction with aerial oxidation[16]. Oxidative cyanide dissolution remains the key industrial gold leaching process[17,18] and is commonly used because of its relatively low cost and great effectiveness. The main advantages are the selectivity of free cyanide for gold dissolution and the high stability of the gold-cyanide complexes.[19,20] Recently, thiourea, thiosulfate, chlorine and acid leaching techniques have been developed as an alternative to cyanide, but none of these has yet gained industrial application.[21,22]

In alkaline cyanide solutions, the aerial oxidation of gold is a prerequisite for its dissolution, an electrochemical process. The gold dissolution in cyanide-containing solutions may be limited due to the passivation of the gold surface, resulting in the formation of gold oxide and sub-oxide surface species.[23,24] The gold dissolution oxidative process in cyanide-containing solution is a complex mechanism, which can be affected by a number of influential parameters such as the cyanide concentration, availability of oxygen at the solid-liquid interface, the presence of ions other than CN^- in solution, pH and temperature.[25,26] Many studies have been carried out to investigate these factors, but there is less information regarding the behaviour of gold at the nanoscale.

In this article, the dissolution of citrate-capped gold nanoparticles (AuNPs) in cyanide-containing solution is assessed both as nanoparticle ensembles and at the single particle level. The analysis of the AuNPs as an ensemble was carried out through cyclic voltammetry of random arrays of AuNPs drop-cast onto a glassy carbon electrode surface (AuNPs-GCE), while the oxidation of single AuNPs was performed using the electrode-particle collision method.[27-32]

The electrode-particle collision method (hereafter referred to as "impact-chemistry") is a powerful technique that allows the study of the electrochemical behaviour of single particles. With this technique, it is possible to characterize individual nanoparticles, and to study their reactivity in various solutions. In the electrode-particle collision method, the nanoparticles are suspended in solution and, by virtue of their Brownian motion, they randomly collide with the surface of a microelectrode immersed in solution. Upon collision, the nanoparticles may for instance adsorb, dissolve and/or promote various reactions, from catalytic to ion insertion, and complex ion formation.[27,33-35] The stochastic collisions of the nanoparticles against the electrode surface typically result in spikes or steps in the background current recorded at the microelectrode.

The oxidative dissolution of gold through impact-chemistry has been given proof-of-concept in the presence of bromide (Br^-).[36]

[a] Department of Chemistry, Physical and Theoretical Chemistry Laboratory, Oxford University, South Parks Road, Oxford, OX1 3QZ, UK.
E-mail: richard.compton@chem.ox.ac.uk
Fax: +44 (0)1865 275410
Tel: +44 (0)1865 275957
[b] Department of Materials, Oxford University, Parks Road, OX1 3PH, UK.

Electronic Supplementary Information (ESI) available.
See DOI: 10.1039/x0xx00000x

Now at the Laboratory for Bioanalytics and Clinical Chemistry, University of Manitoba, Winnipeg, Canada
† Now at the School of Engineering and Applied Sciences, Harvard University, Cambridge, MA, USA

View Article Online
DOI: 10.1039/C8CP05154B

Moreover, oxidative dissolution of AuNPs have been successfully detected and characterized using the impact-chemistry method in aqueous 0.1 M HCl.[37] Sticking probabilities have also been measured.[38]

In this work, the analysis of the shape, charge, current, duration and frequency of a statistically relevant number of single collision events has been carried out in order to understand the reactivity and the mechanism of gold dissolution at the nanoscale in cyanide-containing solution and to contrast this with the nanoparticle ensemble behaviour. Clear insights into the kinetics and mechanism of the process at the single particle level emerge.

Experimental

Chemicals and Reagents

Potassium cyanide (KCN, ≥97.0%) and sodium hydroxide (NaOH, ≥97.0%) were obtained from Sigma Aldrich UK and used as received. Cyanide solutions were prepared in 10 mM NaOH to avoid the formation and volatilization of HCN during the experiment.[39] All the solutions were prepared using nanopure water with resistivity not less than 18.2 MΩ cm at 298K (Millipore, US). All solutions were degassed thoroughly with pure nitrogen stream (BOC Gases plc, UK) before measurement. Citrate-capped gold nanoparticles were obtained commercially, nominally 12 nm, 20 nm (both Nanocomposix Inc., San Diego, US) and 60 nm (Nanopartz Inc., Loveland, US) particle sizes. According to the Nanocomposix's product specification, the main ingredients of their nanoparticles are Au (0.005 % mass), sodium citrate dihydrate (5.8×10^{-5} % mass) and water (>99 % mass). For the Nanopartz product the ingredients are Au (0.005 % mass), citrate, "18 MEG DI water" and residual chemicals (<0.1 % mass). Note that no information provided by Nanopartz regarding the composition of this residual chemical. Nanocomposix declares that their manufacturing process of the gold nanoparticles allow for the "washing" of the colloid with buffer solutions "to remove all residual reactants", resulting in a high purity solution that contains only gold nanoparticle and surface capping agent (citrate).

Electrochemical Procedure

Electrochemical experiments were performed in a thermostatted (25 ± 1 °C) Faraday cage using a μAutolab III potentiostat (Metrohm-Autolab BV, The Netherlands). A standard three-electrode setup was used by employing a saturated calomel electrode (SCE, BASi, Japan) as the reference electrode, a 0.5 mm diameter platinum wire (Goodfellow Cambridge Ltd., UK) as the counter electrode and a glassy carbon (GCE, 1.49 ± 0.01 mm radius, CH Instruments Inc., US) as the working electrode. Prior to each measurement, a GCE was polished using nanopure water-alumina slurry of decreasing particle sizes (1.0, 0.3 and 0.05 mm, Buehler, IL, UK) on soft lapping pads, followed by drying with a pure nitrogen stream.

Impact-chemistry. All chronoamperometric measurements were recorded using a 7.0 μm carbon microdisc electrode (ALS, Japan) with platinum and SCE as reference and counter electrodes, respectively. This three-electrode setup was immersed in the solution containing of ca. 42.0 pM AuNP and 10 mM NaOH. All chronoamperograms were recorded at potential of 0.3 to 1.2 V vs. SCE for 25 s. An electrochemical cell was placed inside a double Faraday cage, where an in-house built low noise potentiostat was used with a 100 Hz Bessel-type low pass filter.[40] Note that the potentiostat used in this work accurately conserves the charge transferred due to a particle-impact process despite possible distortion of the spike shape.[27,41] The analogue-to-digital and digital-to-analogue conversion was provided by a USB-6003 DAQ (National Instruments, TX, US). The control of these devices were performed by a script written in Python 2.7 with a graphical user interface and real-time electrochemical data visualization based upon the packages provided in the Enthought Tool Suite (Enthought, TX, US). Analysis of impact-chemistry spikes was performed using "SignalCounter" program.[42]

Transmission Electron Microscopy (TEM). A JEOL JEM-3000F field emission gun instrument, with an accelerating voltage of 300 kV, was used to determine the size of the AuNP. For sample preparation, holey carbon grids were modified by drop casting the AuNP suspension and allowing them to dry. Different areas of the grid were imaged to ensure a representative view of the sample. ImageJ software (National Institute of Health, US) was used to size the AuNP recorded on the micrographs.

Scanning Electron Microscopy (SEM). A JEOL JSM-6500F, with an accelerating voltage of 5 kV, was used to study the aggregation/agglomeration states of the AuNP in drop cast film. A glassy carbon (GC) plate was used as an electron imaging substrate. The preparation of the GC plate involved treatment with aqua-regia in order to provide a clean surface, rinsing with nanopure water and followed by the polishing procedure as described above.

Dynamic Light Scattering (DLS). A Malvern Zetasizer Nano ZS instrument was used to measure the hydrodynamic diameter of the AuNP. Each sample was diluted with 10 mM NaOH and filtered using a sterile Whatman 0.2 μm filter to remove any dust particles or other large contaminants, before placed in a disposable solvent-resistant microcuvette with a path length of 10 mm. Prior to the measurement, each sample was equilibrated at 25 °C inside the instrument for two minutes. Three sets of 12 light scattering measurements were taken using 633 nm He-Ne laser and averaged to give three size distributions for the nanoparticles. Zetasizer Software from Malvern (Malvern Panalytical Ltd., Malvern, UK) was used to analyze the data.

Nanoparticle Tracking Analysis (NTA). NTA measurements were performed with a NanoSight LM10 (NanoSight, Amesbury, UK), equipped with a sample chamber and a 642 nm laser. The sample suspension was diluted 100 times, with respect to the initial concentration of ca. 42.0 pM used for the impact-chemistry experiment, in order to get a concentration of particles of the order of 10^9 particles ml^{-1} to minimize the noise of the analysis. The samples were injected into the sample chamber with sterile syringes (BsD Discardit II, US) and the absence of air bubbles was ensured. All measurements were performed at room temperature. Three runs of 60 s each at three different portions of the samples were measured with automatic setting at 30 frames per second.

View Article Online
DOI: 10.1039/C8CP05151B

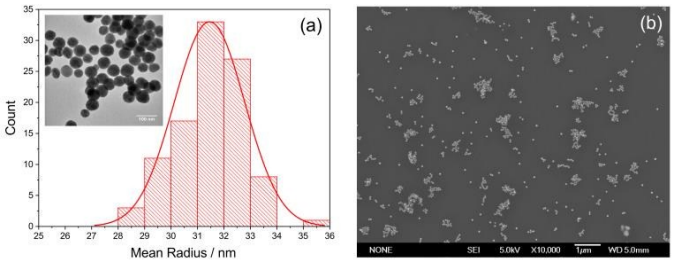

Figure 1. (a) Statistical distribution of the AuNP radius size (inset: TEM micrograph of the AuNP). (b) SEM micrograph of AuNP showing the aggregation/agglomeration state of the particles.

Zeta Potential. A Malvern Zetasizer Nano ZS Malvern (Malvern Panalytical Ltd., Malvern, UK), with an irradiation wavelength of 633 nm (He-Ne laser), was used to study the stability of colloidal dispersions of the AuNP in nanopure water and cyanide-containing solutions. Disposable folded capillary cells were filled with the AuNP suspension to be analyzed and measured.

UV-vis Spectroscopy. A Shimadzu UV-1800 with 20 µl High Precision Quartz Cells (Hellma Analytics, Germany) was used to measure the stability of the AuNP in different HCl-KCl concentrations. In all cases, a baseline correction was performed prior to the measurement and the absorbance was recorded from 800-450 nm. An 700 µl of the AuNP suspension was mixed with 800 µl of various NaOH concentrations ranging from 10 to 100 mM.

Results and discussion

This section outlines the characterization and electrochemical measurements of gold nanoparticles in cyanide-containing solutions. The voltammetry studies are conducted at the nanoparticle ensemble and at the single particle levels. Studies of nanoparticle ensembles are undertaken with cyclic voltammetry of drop casted AuNPs onto a GCE surface (AuNPs-GCE). The presence of a gold stripping peak, the effect of the scan rate and the surface concentration, the maximum peak charge during successive scans, and the percent conversion of oxidized AuNP are investigated. Following this, particle impacts in a suspension of single particles were undertaken, and the observed spikes in the current-time trace were integrated and sized. Finally, the AuNPs oxidation, and dissolution mechanism and rate are discussed.

Characterization of Gold Nanoparticles

Initially, the physical characterization of the commercially sourced "nominally 60 nm" diameter citrate-capped gold nanoparticles (AuNPs) was conducted using transmission electron microscopy (TEM), scanning electron microscopy (SEM), dynamic light scattering (DLS), nanoparticle tracking analysis (NTA), zeta potential measurement (ZP) and UV-vis spectroscopy (UV-vis).

As shown in Figure 1a, the AuNPs exhibit a spheroidal shape with an average diameter size of 62.9 ± 2.7 nm, as extracted from TEM micrographs of 100 particles, in accordance with the manufacturers size specification of "nominally 60 nm". The SEM analysis of the AuNPs suspension drop cast onto a GC plate reveals numerous clusters due to particle aggregation/agglomeration (Figure 1b). This can cause incomplete stripping oxidation of the AuNP.[43,44] Therefore, these effects must be considered when the study of ensemble AuNPs, through drop casting AuNPs onto GCE surface (AuNPs-GCE), is undertaken (see below).

DLS was undertaken to measure the hydrodynamic diameter of the AuNPs. This analysis revealed that the average hydrodynamic diameter of the particles is 64.0 ± 0.3 nm (Figure SI.1a). The polydispersity index for all measurements was 0.07 ± 0.01, indicating that particles size were closely monodispersed. The NTA analysis exhibited an average size of 65.0 ± 0.9 nm (Figure SI.1b). Zeta potential analysis showed the values of -43.6 ± 2.3 mV, -45.6 ± 1.4 mV and -36.7 ± 0.7 mV for the overall electrokinetic potential of each sample of AuNPs in nanopure water, in 10 mM NaOH and in 50.0 mM KCN + 10 mM NaOH, respectively (Figure SI.1c).

To gain information about the stability of the AuNP in cyanide-containing solution, time dependent UV-Vis spectroscopy was performed. Each sample was deaerated thoroughly with high purity nitrogen flow prior to the measurements. Note that in this context, "stability" means that the AuNPs are resistant to aggregation and agglomeration. The stability of the AuNPs can be monitored using UV-Vis spectroscopy due to the presence of a surface plasmon resonance absorption peak, which results in the observation of a maximum absorbance at the characteristic wavelength of 520-535 nm, depending on the nanoparticle size.[45] As shown in Figure 2, the AuNPs showed higher stability in the solution containing of 5.0 mM KCN than 25.0 and 50.0 mM KCN, over the time range studied. The result suggests that AuNPs stability in colloidal phase decreased by increasing the CN^- concentrations.

Electrochemical Analysis of AuNPs-GCE

The redox properties of ensembles of AuNPs were assessed by voltammetry performed at a AuNPs-GCE immersed into a solution of 5.0 mM KCN + 10 mm NaOH. First, an unmodified-GCE was immersed in solution of 5.0 mM KCN + 10 mM NaOH and cyclic voltammetry (CV) was recorded by sweeping the potential from -0.6 V (vs. SCE) to 0.5 V at scan rate of 0.1 V s^{-1}. In the absence of AuNPs (Figure 3, solid black line), the voltammetric response of an unmodified-GCE did not exhibit any oxidative features in the potential range studied. Subsequently, the GCE surface was modified by drop casting ca. 20 µl of the AuNPs suspension, resulting in approximately one-monolayer surface coverage that corresponded to ca. 5 x 10^8 particles (SI.1 Calculation Detail). Then, analogous CV experiments as with the unmodified-GCE were performed.

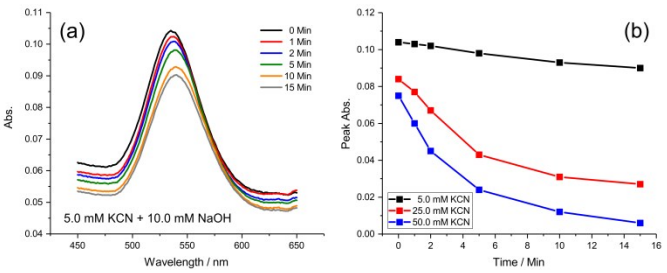

Figure 2. (a) UV-vis spectra of the AuNPs in a solution of 10 mM NaOH containing 5.0 mM KCN. (b) Distribution plot of peak absorbance against time at various KCN concentrations.

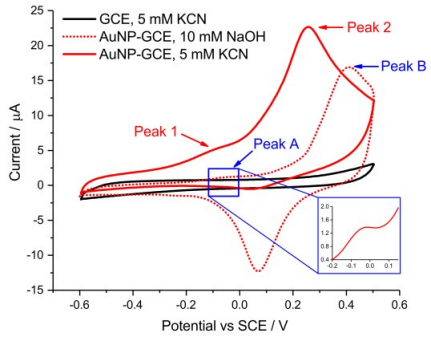

Figure 3. Voltammograms of the unmodified-GCE immersed in 5.0 mM KCN (solid black line) and the AuNPs-GCE immersed in 10 mM NaOH (red dotted line) or in 5.0 mM KCN (red solid line).

In the absence of CN^- (Figure 3, dotted red line), two oxidative peaks in the first forward scan of the voltammogram were observed at peak potentials of -0.05 V and 0.40 V, respectively. These peaks have been assigned to the oxidation of gold to gold hydroxide $Au(OH)_{ads}$ (hereafter referred to as "peak A") and to gold oxide Au_2O_3 (hereafter referred to as "peak B").[46-48] The $Au(OH)_{ads}$ species is formed due to reaction of AuNPs with OH^- from the electrolyte (Reaction 1). A further oxidation process leads to the formation of Au_2O_3 layers at more positive potentials (Reaction 2). The peak current of Au_2O_3 species increased linearly as a function of the scan rate, suggesting a surface-controlled process involving the passage of a constant charge within a fixed potential range.

$$Au\ (s) + OH^- \longrightarrow AuOH\ (ads) + e^- \quad \text{(Reaction 1)}$$

$$2Au\ (s) + 3H_2O \longrightarrow Au_2O_3 + 6H^+ + 6e^- \quad \text{(Reaction 2)}$$

In the presence of 5.0 mM KCN, the AuNPs-GCE exhibits two oxidative features at peak potentials of ca. -0.10 V and ca. 0.28 V vs. SCE (Figure 3, solid red line). These peaks are reported to correspond to the formation of $AuCN_{ads}$ (hereafter referred to as "peak 1") and $Au(CN)_2^-$ (hereafter referred to as "peak 2"), respectively, which are formed through the following reaction pathways.[49-51]

$$Au\ (s) + CN^-(aq) \rightleftharpoons AuCN^-(ads) \quad \text{(Reaction 3)}$$

$$AuCN^-(ads) \rightleftharpoons AuCN\ (ads) + e^- \quad \text{(Reaction 4)}$$

$$AuCN\ (ads) + CN^- \rightleftharpoons Au(CN)_2^- \quad \text{(Reaction 5)}$$

According to Kirk *et al.*[49], the reaction occurring at peak 2 is consistent with the reactions 3 to 5, with reaction 5 as the rate-determining step. Meanwhile, the reaction at peak 1 involves the same dissolution scheme as for peak 2, but with reaction 4 likely to be the rate-determining step. The dissolution of gold in cyanide-containing solution through the reaction pathways described above is suggested to be terminated at potentials more positive than potential of peak 2 by the formation of $Au(OH)_3$.[49] It has been suggested that $AuOH_{ads}$ species (reaction 1) can potentially block the reaction with CN^- causing gold passivation[50,51], whilst the adsorption of CN^- facilitates the dissolution of the AuNPs and leads to the complexation between AuNP and CN^-, promoting the oxidative dissolution of AuNPs. The dicyanoaurate(I) complex ion, $Au(CN)_2^-$, is known for its high stability. It has an equilibrium constant value for the formation of a complex Au-CN estimated in the range of 1.0×10^{37} to 2.8×10^{39}.[20]

The coverage of AuNPs drop casted onto the GCE surface was varied in the range of 0.1 to 1.0-monolayers. Analogous measurements were performed to these as described above. The results demonstrate that the peak current of peak 2 increased monotonically on increasing surface coverage in the range studied (Figure SI.2). This is attributed to the greater number of nanoparticles readily available for complexation with CN^- and subsequent oxidation. A one-monolayer surface concentration was selected for further experiments, in particular to calculate the total charge of the peak 2 after successive scans and to determine the percent conversion of the oxidized AuNPs (see below).

The effect of the scan rate at different fixed CN^- concentrations was evaluated. A one-monolayer AuNPs-GCE was immersed into solutions of 10 mM NaOH containing five different CN^- concentrations, ranging from 1.0 to 50.0 mM. Voltammograms were recorded by sweeping the potential from -0.6 V to 1.0 V vs. SCE at a scan rate of 0.02 to 0.2 V s^{-1}. The peak currents were determined by applying a polynomial fit (typically of order 6) to extract the signal from the baseline. The peak currents increased linearly with scan rate, consistently for all CN^- concentrations (Figure SI.3). The linear dependence of the peak current on the scan rate suggests that the oxidation is a surface-controlled process. As shown in Figure 4a, the first scan of CVs recorded at a scan rate of 0.1 V s^{-1} shows that the peak current values of peak 2 increased linearly on increasing the CN^- concentration. However, the peak potential corresponding to the oxidation of peak 2 was shifted to more negative potentials by increasing CN^- concentrations (Figure 4b). This likely arises from an increased rate of reaction at higher levels of CN^-, leading to fuller stripping at lower potentials.

Finally, the charges associated with peak 2 were measured to calculate the percent conversion of oxidized AuNPs. The percent conversion is determined as a ratio between the experimental charges of the peak 2 recorded from the CVs and the expected charges for complete particle oxidative dissolution (SI.1 Calculation Detail). To determine the total experimental charge of peak 2, a one-monolayer AuNPs-GCE was immersed into a solution of 10 mM NaOH with five different CN^- concentrations, and then a multiple cycle-CV was performed until the oxidative features were no longer discernible (Figure SI.4). The total charge from successive CV scans was determined by integrating the area of peak 2, until no oxidative features were observed. The charge expected from the number of

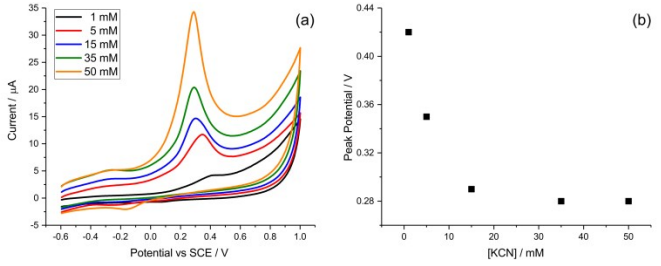

Figure 4. (a) The first forward scans of the AuNPs-GCE immersed into a 10 mM NaOH containing various CN^- concentrations at scan rate of 0.1 V s^{-1}. (b) Plot of peak potential of peak 2 against different CN^- concentrations.

drop casted AuNPs was estimated to be ca. 600 μC (SI.1 Calculation Detail). The ratio between experimental and expected charge values, assuming one electron was transferred per gold atom, was then considered as the yield of oxidized AuNPs. The percent conversions of ensemble AuNPs were found to be small, ranging from ca. 1.6% to 7.8% throughout the five different CN^- concentrations studied (SI.1 Calculation Detail). These small percentages correspond to the incomplete stripping behaviour of the AuNPs, which is strongly affected by the aggregation/ agglomeration states of particles[52,53] as verified by SEM (Figure 1b).

Impact-Chemistry Analysis of Single AuNP

In this section, we report the spike shape, charge, current, duration, frequency and oxidation rate resulting from the impact-chemistry experiments. The results are obtained from stochastic single collision events of individual AuNPs with a potentiostated carbon microelectrode immersed in solution and polarized at a fixed potential.

A 7.0 μm diameter carbon microelectrode was immersed into a solution containing 10 mM NaOH and a ca. 42.0 pM AuNPs suspension (ca. 1.8×10^{10} particles ml^{-1}). Chronoamperograms were then recorded by applying a fixed potential ranging from 0.3 to 1.1 V for 25 s. A series of chronoamperograms were recorded in order to obtain at least 100 spikes for the analysis. First, in the absence of CN^- in the system, a featureless continuous time-current transient was observed at all potentials studied (Figure SI.5a). Next, this procedure was repeated in the absence of AuNPs, in which the system contained 10 mM NaOH and five different CN^- concentrations ranging from 1.0 to 50.0 mM. Featureless chronoamperograms were also observed in this case. (Figure SI.5b)

Subsequently, both ca. 42.0 pM AuNP and particular CN^- concentrations were introduced together in the system and analogous experiments conducted. Figure 5 depicts four representative chronoamperograms with their zoomed spikes (inset) at an applied potential of 1.0 V. The resulting spikes features in the transient current are attributed to individual AuNPs stochastically colliding with the microelectrode surface in the presence of CN^-, consistent with the oxidation of AuNPs occurring

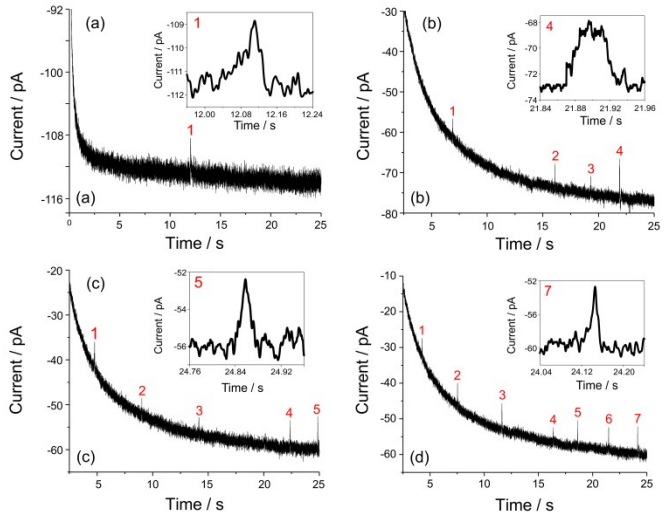

Figure 5. Representative chronoamperograms of microelectrode immersed in a solution containing ca. 42.0 pM AuNPs and (a) 1.0 mM, (b) 5.0 mM, (c) 15.0 mM and (d) 50 mM CN^- at potential of 1.0 V.

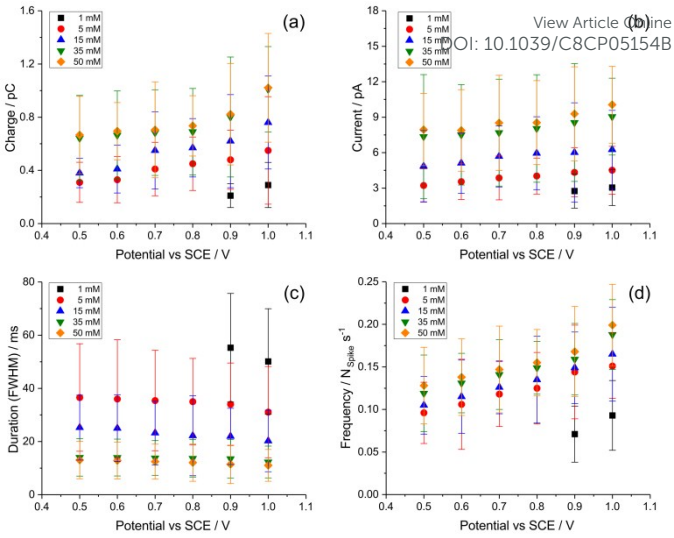

Figure 6. Linear relationship of average spikes (a) charge, (b) current, (c) duration at full width at half-maximum (FWHM) and (d) frequency and CN^- concentrations with different potentials.

through surface complexation with CN^- and subsequent oxidative dissolution reaction. Bigger spikes are seen in higher CN^- concentration (see below). Smaller nanoparticles (12 and 20 nm) gave features too small to detect (Figure SI. 6).

Chronoamperograms at nine different potentials, in the range of 0.3 to 1.1 V, were measured to investigate the potential dependency of the impact-chemistry. As shown in Figure 6, the spike features were exclusively observed only at potentials greater than 0.4 V and less than or equal to 1.0 V; no spikes were seen above 1.0 V. For 1.0 mM CN^-, spikes were only seen at potentials greater than 0.8 V (Figure 6, square black symbol). For the other CN^- concentrations, the average charge and current per spike tends to a plateau on increasing the potential to a maximum of 1.0 V (Figure 6a, b). The absence of spikes at potentials lower than 0.5 V is attributed to insufficient overpotential for the particle oxidation. Meanwhile, the absence of spikes at potentials higher than 1.0 V is probably due to the formation of nonconductive hydroxide or oxide layers on the surface of the individual AuNPs, which inhibit the particle dissolution.

The average spike duration was determined as a full width at half-maximum (FWHM), the width of individual spike at half of the maximum current amplitude. The average duration was found to be shorter with increasing CN^- concentrations, namely ca. 30 ± 17 ms, 20 ± 12 ms, 12 ± 6 ms and 11 ± 6 ms for 5.0, 15.0, 35.0 and 50.0 mM, respectively (Figure 6c). In addition, the spike shape was found to be independent of the CN^- concentration. The shorter impact-chemistry duration implies a faster reactivity of the individual AuNPs in higher CN^- concentrations, leading to a quicker dissolution reaction (see below).

The impact-chemistry is stochastic in nature, thus the number of collision events observed per one chronoamperogram may vary. The average impact frequency, number of individual collision event per second, was found to be roughly constant with increasing CN^- concentrations and applied potentials (Figure 6d). This suggests that the frequency of impact-chemistry is essentially independent of CN^- concentration, at least in the concentration range studied.

View Article Online
DOI: 10.1039/C8CP05154B

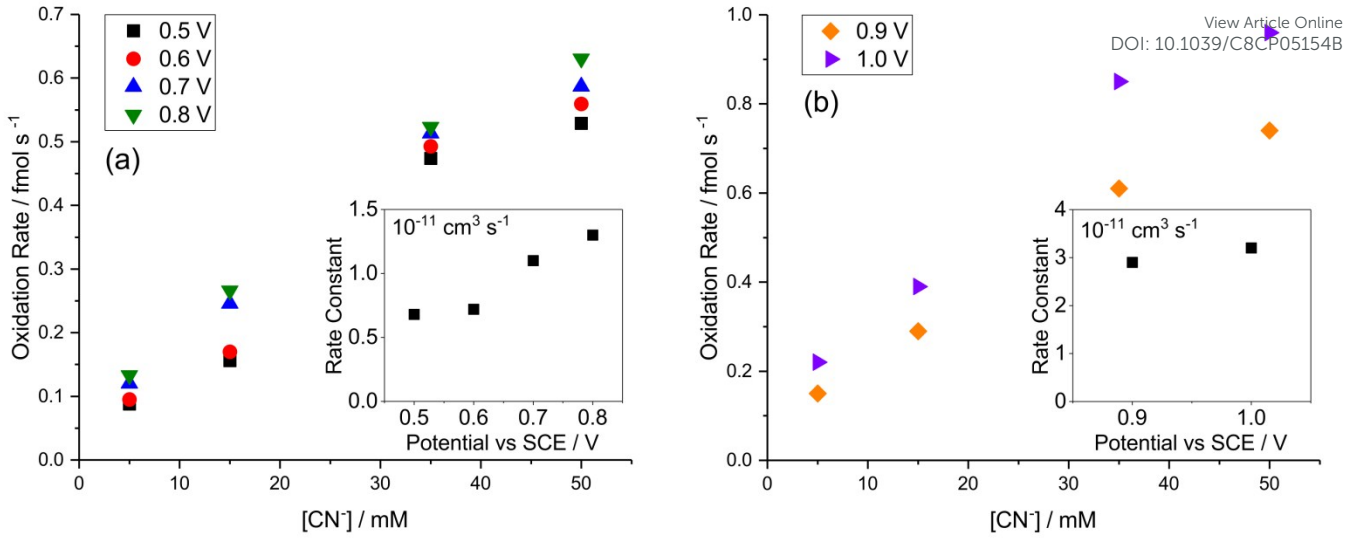

Figure 7. The oxidation rate of the individual AuNPs. Linear relationship between oxidation rate and CN^- concentrations at applied potential of (a) 0.5 V to 0.8 V. (b) Greater than 0.8 V. The rate constant is reported (inset).

The expected charge from the oxidation of the average AuNP, assuming a one-electron transfer, was calculated to be ca. 1.1 pC (SI.1 Calculation Detail). The ratio between the experimental and expected charge values was considered as the percent conversion of the average AuNP. The percent conversion was calculated to be ca. 94 ± 5% in the presence of 35.0 mM CN^- or higher (Table SI.1). The nearly complete oxidation process at 35.0 mM CN^- or higher, also suggests the near complete gold particle dissolution into CN^- solution.

Assuming a rate law of the form: rate / mole s^{-1} = k $[CN^-]$, as suggested by the linearity of Figure 7 (a) and (b), the rate constant, k / cm^3 s^{-1}, can be inferred and the values are shown as insets in the figures. For potentials in the range of 0.5 to 0.8 V, the rate constant is approximately independent of potential, whilst for the range of 0.8 to 1.0 V it is higher (Figure 7(b), inset). A comparison between Figure 3 and Figures 6 and 7 shows that significantly higher potentials are required for particle oxidation in the case of impact-chemistry over ensembles. This likely reflects partly a high electrical contact resistance in the case of solution phase impacts as compared to dried drop casted deposits as noted in related cases through direct measurement of contact resistance via "bridging" impacts[54], coupled with a possible loss of driving force for electron transfer resulting from the capping agent (citrate) on the particles and also possibly from oxide layer formation. Assuming a significant contact resistance, the two kinetic regimes evidenced in Figure 7 might be tentatively attributed to the change in rate-determining step identified by Kirk *et al.*[49] and discussed above on the basis of reaction 3, 4 and 5.

The complete or near complete dissolution of the single AuNPs for high CN^- concentrations contrasts strongly with the corresponding behaviour seen for AuNP ensembles as reported above. As an ensemble, the AuNPs did not achieve a complete oxidation, at least partly due to the particle aggregation/agglomeration, and thus the gold dissolution is limited. In contrast, impact-chemistry experiments revealed that a nearly complete oxidation process occurred at concentration of 35.0 mM CN^- and higher, at a potential of 1.0 V. The data in Figure 7b shows CN^- is involved in the rate-determining step and since the reaction is oxidative the CN^- likely pre-adsorbs on the AuNP surface prior to oxidative dissolution.

Conclusions

The electrochemical dissolution behaviour of AuNPs was evaluated at the ensemble and at the single particle level in cyanide-containing solutions, through cyclic voltammetry and impact-chemistry experiments, respectively. The CV experiments of the nanoparticles ensemble exhibited incomplete oxidation of the AuNPs. In contrast, the impact-chemistry experiments revealed that a nearly complete oxidation of the AuNPs was achieved at greater than or equal to 35 mM CN^- with an applied potential of 1.0 V. Moreover, by studying single particles, the oxidation of the AuNPs was shown to be controlled by a pre-adsorption step of CN^- onto the surface of individual AuNPs before the electron was transferred. This further understanding of the AuNPs dissolution and their reactivity in cyanide-containing solution is of great importance for the optimization of the gold nanoparticles recovery and refinery through the cyanidation process.

Conflicts of interest

There are no conflicts to declare.

Acknowledgements

A.L.S. thanks the Indonesian Government through an Indonesia Endowment Fund Scholarship (S-3453/LPDP.3/2016) for funding. S.K. thanks the support from the European Commission under the Marie Curie Program (grant number 702009). The content reflects only the authors' views and not the views of the European Commission. H.M.A. Amin thanks DFG for funding (No. AB 702/1-1). The research leading to these results has received funding also from the European Research Council under the European Union's Seventh Framework Program (FP/2007-2013)/ERC Grant Agreement No. 320403.

PCCP ARTICLE

References

1. A.S.K. Hashmi, *Top. Organomet. Chem*., 2013, **44**, 143-164.
2. R. Ciriminna, E. Falletta, C. Della Pina, J.H. Teles, M. Pagliaro, *Angew. Chemie-Int. Ed.*, 2016, **55**, 14210-14217.
3. G. J. Hutchings, *Catalysis Today*, 2014, **238**, 69-73.
4. W. Jin, G. Maduraiveeran, *Trends Environ. Anal. Chem.,* 2017*,* **14**, 28-36.
5. M.E. Kyriazi, D. Giust, A.H. El-Sagheer, P.M. Lackie, O.L. Muskens, T. Brown, A.G. Kanaras, *ACS Nano*., 2018, **12**, 3333-3340.
6. Y. Il Yoon, X. Pang, S. Jung, G. Zhang, M. Kong, G. Liu, X. Chen, *J. Mater. Chem. B*., 2018, **6**, 3235-3239.
7. S. Campuzano, P. Yáñez-Sedeño, J. Manuel Pingarrón*, Sensors*, 2017, **17**, 866.
8. S. Kuss, E.E.L. Tanner, M. Ordovas-Montanes, R.G. Compton, *Chem. Sci.,* 2017*,* **8**, 7682-7688.
9. P. Pyykkö, Angew. *Chemie-Int. Ed*., 2004, **43**, 4412-4456.
10. R. Sardar, A.M. Funston, P. Mulvaney, R.W. Murray, *Langmuir*, 2009, **25**, 13840-13851.
11. Y.P. Jia, B.Y. Ma, X.W. Wei, Z.Y. Qian, *Chinese Chem. Lett.*, 2017, **28**, 691-702.
12. P. Knittel, O. Bibikova, C. Kranz, *Faraday Discuss*., 2016, **193**, 353-369.
13. A. Assunção, B. Vieira, J.P. Lourenço, M.C. Costa, *RSC Adv*., 2016, **6**, 112784-112794.
14. S. Krishnamurthy, Y.S. Yun, *Chem. Eng. J.,* 2013*,* **214**, 253-261.
15. A.M. Lazim, J. Eastoe, M. Bradley, K. Trickett, A. Mohamed, S.E. Rogers, *Soft Matter*., 2010, **6**, 2050-2055.
16. A.D. Bas, E. Ghali, Y. Choi, *Hydrometallurgy*, 2017, **172**, 30-44.
17. P.D. Kondos, G. Deschênes, R.M. Morrison, *Hydrometallurgy,* 1995, **39**, 235-250.
18. F. Xie, D.B. Dreisinger, *Trans. Nonferrous Met. Soc. China*, 2009, **19**, 714-718.
19. D. M. Mac Arthur, *J. Electrochem. Soc*., 1972, **119**, 672-677.
20. X. Bin Wang, Y.L. Wang, J. Yang, X.P. Xing, J. Li, L.S. Wang, *J. Am. Chem. Soc.,* 2009*,* **131**, 16368-16370.
21. M. Tanriverdi, H. Mordoğan, Ü. Ipekoğlu, *Miner. Eng.,* 2005*,* **18**, 363-365.
22. I. De Michelis, A. Olivieri, S. Ubaldini, F. Ferella, F. Beolchini, F. Vegliò, *Int. J. Min. Sci. Technol*., 2013, **23**, 709-715.
23. A.D. Bas, F. Safizadeh, W. Zhang, E. Ghali, Y. Choi, *Trans. Nonferrous Met. Soc. China,* 2015, **25**, 3442-3453.
24. D. Kirk, F. Foulkes, W. Graydon, *J. Electrochem.*, 1980, **605**, 1962-1969.
25. A. J. McCarthy, *J. Electrochem. Soc*., 1998, **145**, 408.
26. M.I. Jeffrey, I.M. Ritchie*, J. Electrochem. Soc.*, 2000, **147**, 3272.
27. S. V. Sokolov, S. Eloul, E. Kätelhön, C. Batchelor-McAuley, R.G. Compton, *Phys. Chem. Chem. Phys.*, 2017, **19**, 28-43.
28. E. Kätelhön, A. Feng, W. Cheng, S. Eloul, C. Batchelor-McAuley, R.G. Compton. *J. Phys. Chem. C.,* 2016*,* **120**, 17029-17034.
29. M. Pumera, *ACS Nano*, 2014, **8**, 7555-7558.
30. P.H. Robbs, N. V Rees, *Phys. Chem. Chem. Phys*., 2016, **18**, 24812-24819
31. L.K. Allerston, N. V Rees, *Curr. Opin. Electrochem*., 2018, In Press. DOI: 10.1016/j.coelec.2018.03.020
32. K.J. Stevenson, K. Tschulik, *Curr. Opin. Electrochem*., 2017, **6**, 38-45.
33. G. Zampardi, C. Batchelor-McAuley, E. Kätelhön, R.G. Compton, *Angew. Chem.,* 2017, **129**, 656-659.
34. G. Zampardi, S. V. Sokolov, C. Batchelor-McAuley, R.G. Compton, *Chem. - A Eur. J.*, 2017, **23**, 14338-14344.
35. G. Zampardi, J. Thoeming, H. Naatz, H.M.A. Amin, S. Pokhrel, L. Maedler, R.G. Compton, *Small,* 2018*,* 1801765.
36. B.J. Plowman, K. Tschulik, N.P. Young, R.G. Compton, *Phys. Chem. Chem. Phys.,* 2015*,* **17**, 26054-26058.
37. Y.G. Zhou, N. V Rees, J. Pillay, R. Tshikhudo, S. Vilakazi, R.G. Compton, *Chem. Commun*., 2012, **48**, 224-226.
38. Y.G. Zhou, E.J.E. Stuart, J. Pillay, S. Vilakazi, R. Tshikhudo, N. V. Rees, R.G. Compton, *Chem. Phys. Lett*., 2012, **551**, 68-71.
39. K. Chiang, R. Amal, T. Tran*, J. Mol. Catal. A Chem*., 2003, **193**, 285-297.
40. C. Batchelor-McAuley, J. Ellison, K. Tschulik, P.L. Hurst, R. Boldt, R.G. Compton, *Analyst*, 2015, **140**, 5048-5054.
41. E. Kätelhön, E.E.L. Tanner, C. Batchelor-McAuley, R.G. Compton, *Electrochim. Acta*., 2016, **199**, 297-304.
42. J. Ellison, K. Tschulik, E.J.E. Stuart, K. Jurkschat, D. Omanović, M. Uhlemann, A. Crossley, R.G. Compton, *ChemistryOpen*., 2013, **2**, 69-75.
43. S.J. Cloake, H.S. Toh, P.T. Lee, C. Salter, C. Johnston, R.G. Compton, *ChemistryOpen*., 2015, **4**, 22-26.
44. S. V. Sokolov, K. Tschulik, C. Batchelor-McAuley, K. Jurkschat, R.G. Compton, *Anal. Chem.*, 2015, **87**, 10033-10039.
45. X. Huang, M.A. El-Sayed, *J. Adv. Res*., 2010, **1**, 13-28.
46. M. Shamsipur, Z. Karimi, M. Amouzadeh Tabrizi, *Microchem. J.*, 2017, **133**, 485-489.
47. C.M. Welch, M.E. Hyde, O. Nekrassova, R.G. Compton, *Phys. Chem. Chem. Phys.*, 2004, **6**, 3153-3159.
48. L.D. Burke. *Gold Bull*., 2004, **37**, 125-135.
49. D.W. Kirk, F.R. Foulkes, W.F. Graydon, *J. Electrochem. Soc.*, 1978, **125**, 1436.
50. H.K. Lin, X. Chen, *Miner. Metall. Process*., 2001, **18**, 147-153.
51. A.D. Bas, F. Safizadeh, W. Zhang, E. Ghali, Y. Choi, *Trans. Nonferrous Met. Soc. China*, 2015, **25**, 3442-3453.
52. H.S. Toh, K. Jurkschat, R.G. Compton, *Chem.-A Eur. J.*, 2015, **21**, 2998-3004.
53. H.S. Toh, C. Batchelor-McAuley, K. Tschulik, M. Uhlemann, A. Crossley, R.G. Compton, *Nanoscale,* 2013*,* **5**, 4884-4893.
54. X. Li, C. Batchelor-McAuley, L. Shao, S. V. Sokolov, N.P. Young, R.G. Compton, *J. Phys. Chem. Lett*., 2017, **8**, 507-511.

View Article Online
DOI: 10.1039/C8CP05154B